Phytochemistry 242 (2026) 114684

Contents lists available at ScienceDirect

Phytochemistry

journal homepage: www.elsevier.com/locate/phytochem

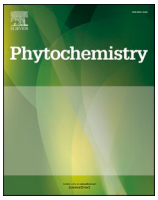

Bioactive specialized metabolites of *Trochila* sp., an endophytic fungus of *Lilium carniolicum*

Mostafa Alilou [a,*], Yun Liu [a], Magdalena Steixner [a], Isidor Happacher [b], Sigrid Beate Abt [b], Ursula Fürnkranz [c], Fabio Gsaller [b], Ursula Peintner [d], Hubertus Haas [b]

[a] Institute of Pharmacy/Pharmacognosy, Universität Innsbruck, Innrain 80-82, 6020, Innsbruck, Austria
[b] Institute of Molecular Biology, Medical University of Innsbruck, Innrain 80-82, 6020, Innsbruck, Austria
[c] Pilzambulatorium, Schlösselgasse 19, Vienna, Austria
[d] Department of Microbiology, Universität Innsbruck, Technikerstraße 25d, 6020, Innsbruck, Austria

ARTICLE INFO

Keywords:
Lilium carniolicum
Liliaceae
Pyridone alkaloids
Trochila sp.
Cenangiaceae
Endophyte
Molecular networking
Antimicrobial activity

ABSTRACT

Bioprospecting of a rice culture of *Trochila* sp. BGP15P7IS3, an undescribed endophytic fungus from *Lilium carniolicum*, resulted in isolation and identification of eleven specialized metabolites, of which four pyridone alkaloid derivatives (**1**, **2**, **4,** and **5**) and a biphenyl derivative (**8**) were identified as previously undescribed natural products. Moreover, two dibenzofuran derivatives, isousnic acid and usnic acid (**9** and **10**) with *S* absolute configuration were reported for the first time from an endophytic fungus. Additionally, the absolute stereochemistry of the previously described compound **7** was determined. The structure of the compounds isolated was established by means of HR-ESI-MS, 1- and 2D NMR, and ECD calculations, as well as utilizing previously published data. All isolates available in sufficient quantities were evaluated for their antimicrobial activity against a plant pathogen, *Botrytis cinerea*, and four human pathogens, *Aspergillus fumigatus*, *Aspergillus flavus*, *Candida albicans*, and *Cryptococcus neoformans*, as well as a human sextually transmitted parasite, *Trichomonas vaginalis*. Compound **3** displayed antifungal activity only against *C. neoformans* with an MIC value of 12.5 μg/mL, and compound **6** exhibited promising antifungal activity with MIC values of 0.39–3.25 μg/mL against all the aforementioned fungal pathogens, and a concentration-dependent growth inhibitory property against *T. vaginalis*. Based on the identification of derivatives, a revised biosynthetic pathway for pyridone-type alkaloids was proposed.

1. Introduction

Plant disease outbreaks continue to pose a growing risk to global food security, biodiversity loss and various socio-economic burdens. These outbreaks have been exacerbated by climate change, resulting in the emergence of new pathogens, increased plant susceptibility to pathogens and/or the rise of multi-drug resistant phytopathogens (Singh et al., 2023). For example, in the case of the phytopathogen *Botrytis cinerea*, which infects more than 200 plant species, the global economic loss caused by it has been calculated from $10 to $100 billion worldwide (Roca-Couso et al., 2021). In addition, several studies have revealed the emergence of some strains of this pathogen that are resistant to conventional fungicides (Sofianos et al., 2023). Similar to plants, antimicrobial resistance (AMR), which occur in various human infectious pathogens, imposes multifaceted issues including increasing health care costs, elevating the death rate, and pushing millions of people into extreme poverty (Aslam et al., 2024). Considering this, there is indeed a huge quest for the discovery and development of new antimicrobial substances to help reduce the burden of AMR in both plant and human pathogens. Among the various sources, microbial natural products stand out as promising and sustainable contributors to drug discovery due to their substantial impact. In recent years, endophytic microorganisms have gained increasing attention as promising sources of bioactive natural products with applications in the agricultural and pharmaceutical industries. These symbiotic microorganisms protect their hosts from the deleterious effects of various biotic (e.g., pathogen attack) and abiotic stresses (e.g., drought, UV radiation), particularly through the production of bioactive molecules (Hardoim et al., 2015; Fadiji and Babalola, 2020).

During a screening campaign for the discovery of novel antimicrobial

* Corresponding author.
E-mail address: Mostafa.alilou@uibk.ac.at (M. Alilou).

https://doi.org/10.1016/j.phytochem.2025.114684
Received 22 June 2025; Received in revised form 19 September 2025; Accepted 21 September 2025
Available online 24 September 2025

natural products from endophytic fungi of plants growing in the alpine region, a potentially new fungal species, *Trochila* sp. BGP15P7IS3, isolated from the leaves of *Lilium carniolicum* Bernh. ex W.D.J.Koch, displayed promising antimicrobial activities against a panel of plant and human pathogens with MIC values ranging from 25 to 50 μg/mL. *L. carniolicum* belongs to the Liliaceae family, with distribution in the southeastern alps, and is a native species to Austria, Italy, and northwestern Balkan Peninsula (https://powo.science.kew.org/). To date, no studies have investigated its endophytes or the specialized metabolites they produce. Thus, this study aims to explore its chemical space by implementing LC-MS/MS and Feature-Based Molecular Networking workflow (FBMN) (Nothias et al., 2020), and to further isolate and identify its active compounds through various chromatographic and spectroscopic methods.

Herein the isolation and characterization of eleven specialized metabolites from *Trochila* sp. BGP15P7IS3 are reported, of which five metabolites (**1**, **2**, **4**, **5**, and **8**) were identified as undescribed natural products, and two metabolites (**9** and **10**) were identified as rare stereoisomers, previously unreported from an endophytic fungus (Fig. 1). All isolated compounds were evaluated for their bioactivities against several plant and human pathogens.

2. Results and discussion

2.1. Identification of Trochila sp. BGP15P7IS3

The phylogenetic analysis (Fig. 2) placed this isolated *Lilium* endophyte unambiguously in the genus *Trochila* Fr. (Leotiomycetes, Helotiales, Cenangiaceae). *Trochila craterium* (DC) Fr. is the type species of the genus *Trochila.* Within the genus, *Trochila* sp. BGP15P7IS3 forms a well-supported lineage with four reference sequences (100 % sequence identity in the rDNA ITS region) originating from endophytes from four different plant species. This indicates that *Trochila* sp. BGP15P7IS3 also represents an endophytic *Trochila* species. The detected relationships indicate that this endophyte very likely has a low host specificity and a broad geographic range: it was detected as endophyte of *L. carniolicum* (Austria, accession No.: PV706653), *Coleostephus myconis* (Portugal, accessionF No.: ON754208.1), *Braya fernaldii* (Canada, accession No.: ON599033.1), *Arabidopsis thaliana* (Spain, accession No.: JX982480.1) and of herbal tea (Iran, accession No. OR936275.1). More thorough taxonomical investigations based on several pure culture isolates are necessary for a formal description of this taxon as a new species of *Trochila*. Species of *Trochila* have, up to the present, been considered as saprotrophs or weak parasites: *Trochila ilicina,* the most closely related known species, was reported as both a weak parasite and a saprotroph of *Ilex aquifolium* L. (Aquifoliales, Aquifoliaceae). *T. laurocerasi* is a parasite on the leaves of *Prunus laurocerasus* L. (family Rosaceae); *T. symploci* is a pathogen on *Symplocos japonica* A. DC. (Ericales, Symplocaceae); *T. colensoi* grows on the leaves of *Cordyline australis* (G.Forst.) Endl. (Asparagaceae); *T. uredinophila* grows on the underside of a *Ficus maxima* Mill. leaf, where it is affected by a rust; and the fungus *T. xishuangbanna* lives on petioles (Gómez-Zapata et al., 2021). Based on our phylogenetic analysis including environmental sequences there is growing evidence for the presence of at least two additional endophytic *Trochila* spp., one from *Brassica napus* L., and one from *Festuca rubra* L., *Ornithopus compressus* L., and *Dalea purpurea* Vent.

2.2. FBMN of the ethyl acetate extract of Trochila sp. BGP15P7IS3

The LC-MS/MS data obtained for 40 subfractions of an EtOAc extract of a rice culture of *Trochila* sp. BGP15P7IS3 were analyzed by MZmine 3.0 (Schmid et al., 2023) and subsequently submitted to the GNPS (Global Natural Product Social Molecular Networking) platform for generating a Feature-Based Molecular Network (FBMN) (Nothias et al.,

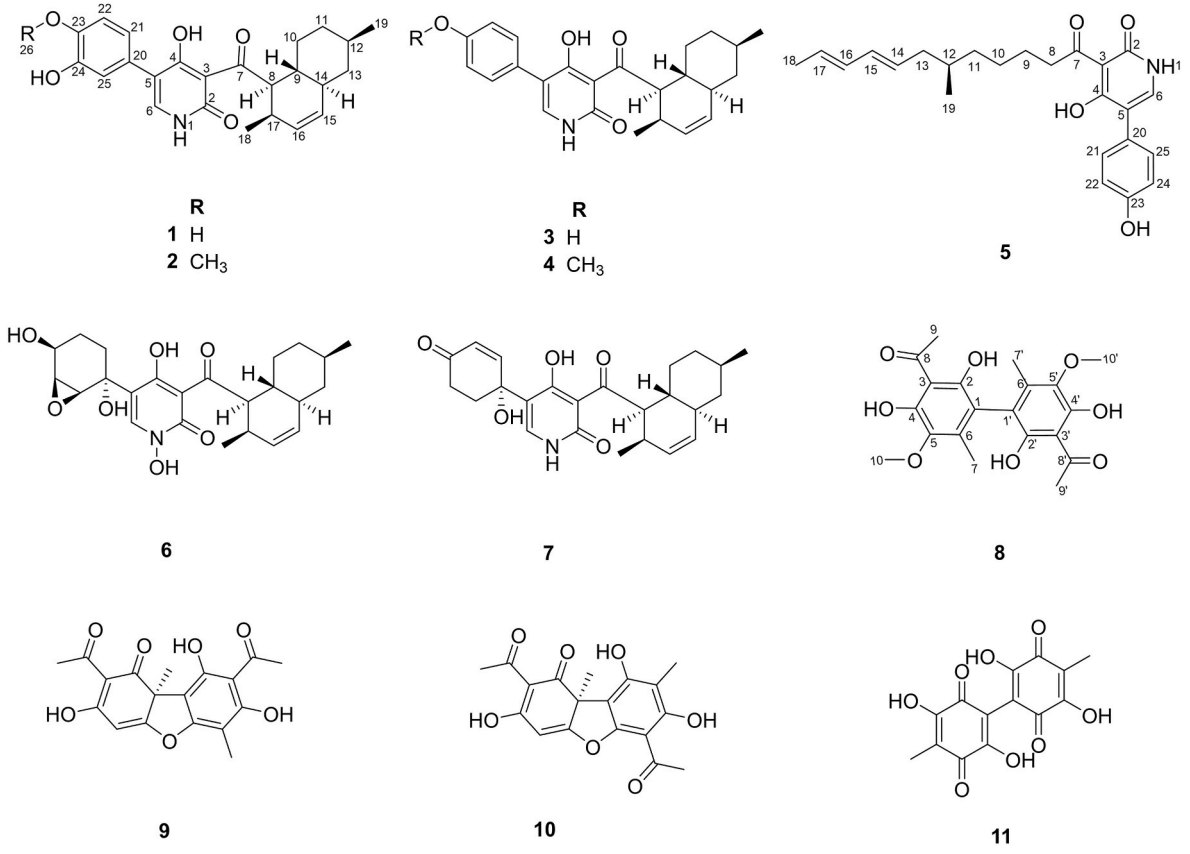

Fig. 1. Structure of the compounds isolated from a rice culture of *Trochila* sp. BGP15P7IS3.

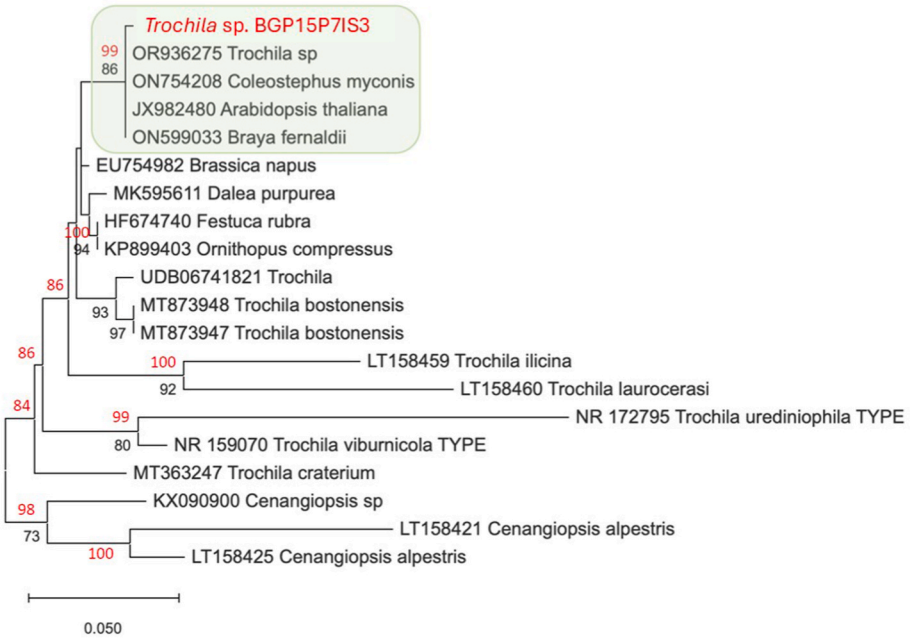

Fig. 2. ML phylogram of *Trochila* rDNA ITS sequences (Cenangiopsis was used as outgroup). Branch support (ML bootstrat and Bayesian PP) are provided above branches. Phylogenetic relationships of the *Trochila Lilium* endophyte based on rDNA ITS sequences. Maximum Likelihood phylogram (log likelihood −1542.04) is shown. T92+G was used as the best model (+G, parameter = 0.2647). Branch support is based on MP bootstraps (100 replicates) in black and Bayesian Posterior Probabilities (2.000000 generations) in red. The dataset included 21 sequences and 376 positions. (For interpretation of the references to colour in this figure legend, the reader is referred to the Web version of this article.)

2020) and annotating compounds present in the extract. The results were visualized using Cytoscape 3.9.1 (Shannon et al., 2003) (Fig. S1). In parallel, SIRIUS (Dührkop et al., 2019) was utilized for further *in silico* dereplication and annotation of potential metabolites. The results indicated the presence of three main classes of compounds including alkaloids, polyketides, and terpenoids (See Fig. S2). Using GNPS, two nodes at *m/z* 345.096 (t_R: 16.43 min) and *m/z* 345.096 (t_R: 15.62 min) could be dereplicated as two known dibenzofurans, isousnic acid (**9**) and usnic acid (**10**). Furthermore, SIRIUS revealed presence of various pyridone-type alkaloids, including nodes with *m/z* 394.2015 (t_R: 14.69 min) and 430.2225 (t_R: 11.53 min), which could be dereplicated as pyridone-type alkaloids, didymellamide B (**3** (Haga et al., 2013), and didymellamide C (**7**, (Haga et al., 2013), respectively (Fig. 3). The structures of both compounds were confirmed using 1 and 2D NMR (See Supplementary Material). Additionally, two known specialized metabolites, *N*-hydroxyapiosporamide (**6**) (Lee et al., 1996) and oosporein (**11**) (Feng et al., 2015) were also isolated. Both classes of compounds have previously been shown to possess strong antimicrobial activities (Haga et al., 2013; Ingólfsdóttr, 2002) and may contribute significantly to the observed bioactivity of the crude extract. Besides the nodes

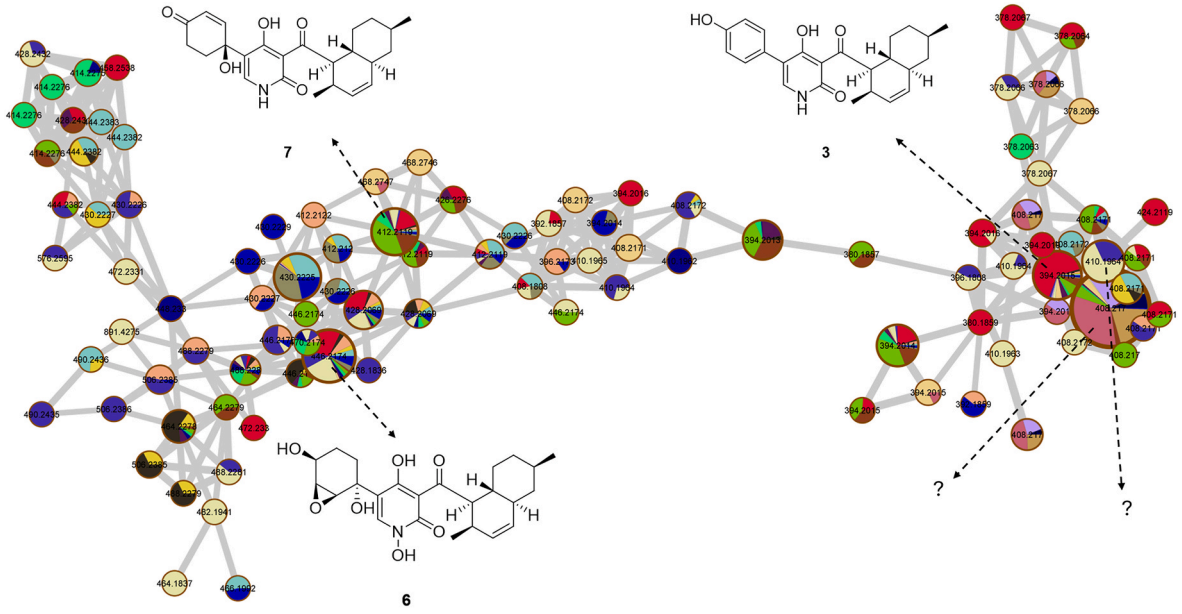

Fig. 3. FBMN of *Trochila* sp. BGP15P7IS3 revealing a cluster of pyridone-type alkaloids. Nodes were annotated using the GNPS spectral library and SIRIUS using MS/MS spectral similarity.

corresponding to known metabolites, several other nodes could not be dereplicated, indicating the presence of potential undescribed derivatives. The fractions containing these compounds were therefore subjected to the targeted isolation.

2.3. Isolation and structural elucidation of compounds isolated

Compound **1** was obtained as a white-brownish solid. Its molecular formula of $C_{24}H_{27}NO_5$ was determined based on HRESIMS data ([M + H]$^+$ *m/z* 410.1959, calcd. for $C_{24}H_{28}NO_5^+$, 410.1962), indicating 12 indices of hydrogen deficiency. The ^{1}H NMR spectrum (Table 1) displayed three aromatic protons [δ_H 6.68 (1H, dd, J = 8.1, 2.1 Hz, H-21), 6.72 (1H, d, J = 8.1 Hz, H-22), and 6.84 (1H, d, J = 2.1 Hz, H-25)], two methyl groups [δ_H: 0.76 (3H, d, J = 7.1 Hz, H-18)] and [δ_H: 0.88 (3H, d, J = 6.5 Hz, H-19)], three olefinic protons [δ_H 7.50 (1H, d, J = 6.1 Hz, H-6), 5.40 (1H, brd, J = 9.7 Hz, H-15), and 5.59 (1H, ddd, J = 9.7, 4.6, 2.5 Hz, H-16)], five methine groups [δ_H: 4.37 (1H, dd, J = 11.4, 5.7 Hz, H-8)], [δ_H: 1.46 (1H, m, H-9)], [δ_H: 1.45 (1H, m, H-12)], [δ_H: 1.78 (1H, m, H-14)], and [δ_H: 2.78 (1H, m, J = 6.2 Hz, H-17)], and three methylene groups [δ_H: 1.80 (1H, m, H-10a) and 0.82 (1H, m, H-10b)], [δ_H: 1.64 (1H, m, H-11a) and 0.95 (1H, m, H-11b)], and [δ_H: 1.67 (1H, m, H-13a) and 0.73 (1H, m, H-13b)]. The ^{13}C NMR together with HSQC spectrum revealed 24 carbon signals, including signals corresponding to the above-mentioned structural units, along with signals for six quaternary carbons (δ_C: 106.8, 175.9, 112.7, 123.8, 144.9, and 144.8) and two carbonyl groups (δ_C: 161.3 and 209.7). The COSY correlations indicated three spin systems, H-9/H-8/H-10b/H-14; from H-17/H-8/H-16/H3-18; H-15/H-14; from H-13b/H-12. Moreover, HMBC spectrum illustrated correlations from H-19 to C-11, C-12, and C-13 (δ_C: 35, 32.5, and 41.3); from H-18 to C-17, C-8, and C-16 (δ_C: 30.6, 51.8, and 131.6); from H-8 to C-7, C-9, and C-17 (δ_C: 209.7, 35.8, and 30.6); and from H-15 to C-9, C-13, and C-14 (δ_C: 35.8, 41.3, and 41.3), collectively indicated the presence of a decalin moiety. Furthermore, the HMBC correlations from H-6 to C-2, C-4, C-5, and C-20 (δ_C: 161.3, 175.9, 112.7, and 123.8) suggested the existence of a 4-hydroxypyridone moiety (Fig. 4). Comparison of the chemical shifts with literature data revealed a strong similarity to didymellamide B (Haga et al., 2013). The main difference between **1** and didymellamide B (**3**) lies in the substitution pattern in the benzene ring, where a typical AA'BB' spin system is substituted by an ABX spin system, assigned to protons H-21, H-22 and H-25. As a result, the planar structure of **1** was elucidated and named as 24-hydroxy didymellamide B (Fig. 1). The NOESY spectrum of **1** displayed correlation between H-9 and H-18, H-8 and H-14, as well as H-14 and H-12, establishing its relative configuration as 8**R*,9**R*,12**R*,14**S*,17**R* (Fig. 5A). Calculating the ECD spectrum at TD-DFT/B3LYP/6-31G(d, p)/CPCM//B3LYP/6-31G(d,p) level in MeOH and comparison with the experimental spectrum resulted in determining the absolute configuration of **1** as 8*R*,9*R*,12*R*,14*S*,17*R* (Fig. 5A).

Compound **2** was obtained as a white-brownish solid. Its molecular formula of $C_{25}H_{29}NO_5$ was determined based on HRESIMS data ([M + H]$^+$ *m/z* 424.2119, calcd. for $C_{25}H_{30}NO_5^+$, 424.2118), corresponding to 12 degrees of unsaturation. Its ^{1}H and ^{13}C NMR spectra (Tables 1 and 2) was identical to that of **1**, except for the presence of a new peak at δ_H 3.78 and δ_C 55.7, characteristic of a methoxy group. Further examination of the HMBC correlations from H-26 (δ_H 3.78) to C-23 (δ_C 147.1) revealed the position of this methoxy group (Fig. 4), establishing its structure as 23-methoxy-24-hydroxy didymellamide B. To further analyze whether this compound was an artefact of the isolation process due to the use of methanol during the isolation steps or was originally present in the extract, LC-MS analysis was performed on the EtOAc extract of the fungus dissolved in THF, as well as on compound **2**. The results clearly confirmed the presence of this compound in the fungal extract (see Fig. S20). This compound revealed a matching ECD spectrum to that of **1**, resulting in establishing its absolute configuration as 8*R*,9*R*,12*R*,14*S*,17*R* (Fig. 5A).

Compound **4** was obtained as a white-brownish solid. Its molecular formula of $C_{25}H_{29}NO_4$ was determined based on HRESIMS data ([M + H]$^+$ *m/z* 408.2169, calcd. for $C_{25}H_{30}NO_4^+$, 408.2169), corresponding to

Table 1
^{1}H (600 MHz) NMR Data of compounds **1**, **2**, **4**, **5**, and **8** (δ in ppm, J in Hz).

Position	1 (DMSO-d_6)	2 (DMSO-d_6)	4 (DMSO-d_6)	5 (CD_3OD)	Position	8 ($CDCl_3$)
1	11.63 d (6.1)	11.61 brs	11.72 brs	–	1	–
2	–	–	–	–	2	–
3	–	–	–	–	3	–
4	–	–	–	–	4	–
5	–	–	–	–	5	–
6	7.50 d (6.1)	7.52 brs	7.59 brs	7.48 brs	6	–
7	–	–	–	–	7	2.14 s
8	4.37 dd (11.4, 5.7)	4.38, dd, (11.4, 5.8)	4.37 dd (11.4, 5.7)	3.18 t (7.4)	8	–
9	1.46 m [a]	1.49 m [a]	1.46 m [a]	1.66 m	9	2.73 s
10 α	1.80 m [b]	1.83 m [b]	1.80 m [b]	1.42 m [a]	10	3.55 s
10 β	0.82 m	0.84 m	0.81 m	1.38 m [a]	1′	–
11 α	0.95 m	0.97 m	0.96 m	1.19 m	2′	–
11 β	1.64 m [b]	1.68 m [b]	1.65 m [b]	1.38 m [a]	3′	–
12	1.45 m [a]	1.46 m [a]	1.45 m [a]	1.50 m	4′	–
13 α	0.73 m [c]	0.75 m [c]	0.75 m [c]	1.90 m	5′	–
13 β	1.67 m [b]	1.73 m [b]	1.67 m [b]	2.07 m	6′	–
14	1.78 m [b]	1.77 m [b]	1.78 m [b]	5.50 m	7′	2.14 s
15	5.40 brd (9.7)	5.39 brd (9.8)	5.39 brd (9.8)	5.96, m	8′	–
16	5.59 ddd (9.7, 4.6, 2.5)	5.59 ddd (9.8, 4.6, 2.7)	5.59 ddd (9.8, 4.5, 2.5)	6.00 m	9′	2.73 s
17	2.78 m	2.78 m	2.79 m	5.55, m	10′	3.55 s
18	0.76 d (7.1) [c]	0.77 d (7.2) [c]	0.77 d (7.2) [c]	1.70 d (6.1)		
19	0.88 d (6.5)	0.89 d (6.5)	0.88 d (6.5)	0.88 d (6.7)		
20	–	–	–	–		
21	6.68 dd (8.1, 2.1)	6.83 dd (8.2, 2.2)	7.38 m	7.28 m		
22	6.72 d (8.1)	6.93 d (8.2)	6.95 m	6.82 m		
23	–	–	–	–		
24	–	–	6.95 m	6.82 m		
25	6.84 d (2.1)	6.90, d (2.2)	7.38 m	7.28 m		
26	–	3.78 s	3.77 s	–		
23-OH	8.92 s	8.90	–	–		
24-OH	8.95 s	–	–	–		

a, *b*, *c*: overlapping signals.

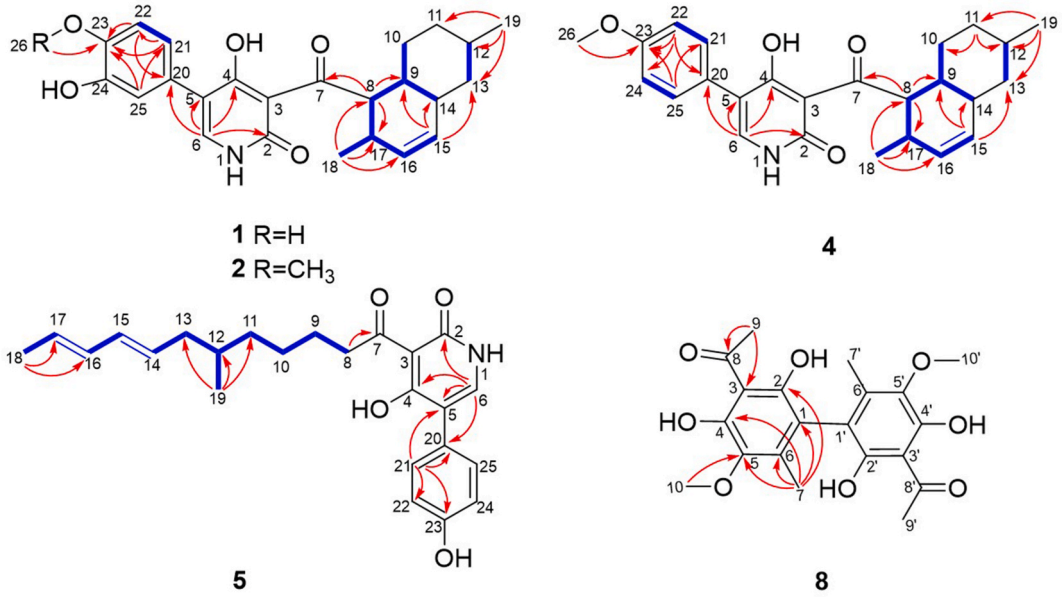

Fig. 4. COSY (blue lines) and HMBC correlations (red arrows) for compounds **1**,**2**, **4**, **5**, and **8**. (For interpretation of the references to colour in this figure legend, the reader is referred to the Web version of this article.)

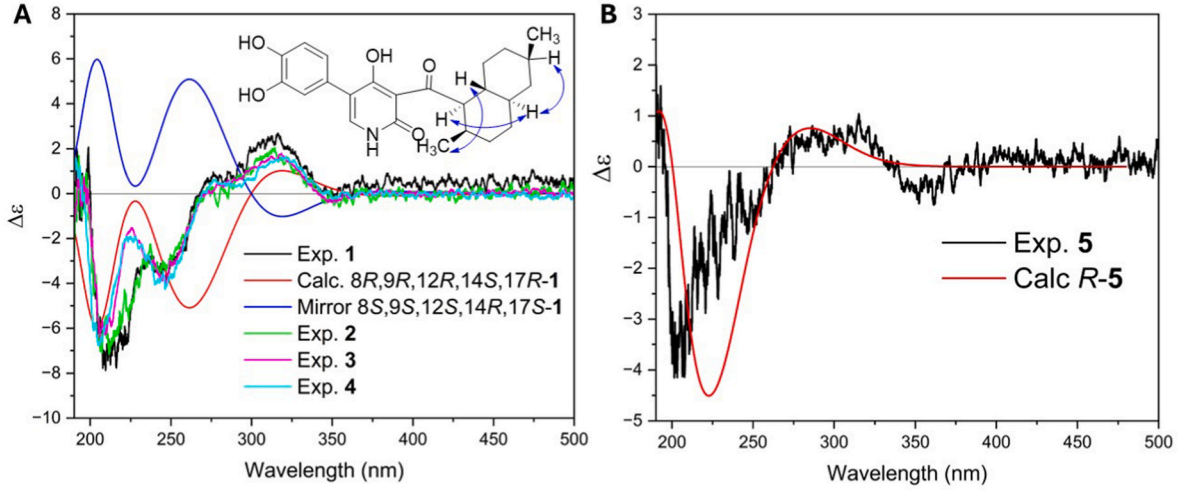

Fig. 5. A) NOESY correlations of **1**, and experimental ECD spectrum of compounds **1**, **2**, **3**, and **4** and calculated ECD spectrum of **1**, B) experimental and calculated ECD spectra of compound **5** in MeOH.

12 degrees of unsaturation. The ^{1}H NMR spectrum of **4** revealed four characteristic aromatic protons [δ_H 7.38 (2H, m, H-21, 25), and 6.95 (2H, m, H-22, 24)], two methyl groups [δ_H: 0.77 (3H, d, J = 7.2 Hz, H-18)] and [δ_H: 0.88 (3H, d, J = 6.5 Hz, H-19)], one methoxy group [δ_H: 3.77 (3H, s, -OCH3)], three olefinic protons [δ_H 7.59 (1H, brs, H-6), 5.39 (1H, dt, J = 9.8, 1.7 Hz, H-15), and 5.59 (1H, ddd, J = 9.8, 4.5, 2.5 Hz, H-16)], five methine groups [δ_H: 4.37 (1H, dd, J = 11.4, 5.7 Hz, H-8)], [δ_H: 1.46 (1H, m, H-9)], [δ_H: 1.45 (1H, m, H-12)], [δ_H: 1.78 (1H, m, H-14)], and [δ_H: 2.79 (1H, m, H-17)], and three methylene groups [δ_H: 1.80 (1H, m, H-10a) and 0.81 (1H, m, H-10b)], [δ_H: 1.65 (1H, m, H-11a) and 0.96 (1H, m, H-11b)], and [δ_H: 1.67 (1H, m, H-13a) and 0.75 (1H, m, H-13b)]. The ^{13}C NMR and HSQC spectrum revealed 24 carbon signals, including signals corresponding to the above structural units and additional signals for five quaternary carbons (δ_C: 106.8, 175.9, 111.2, 125.5, and 158.5) and two carbonyl groups (δ_C: 161.4 and 209.9). Detailed analysis of the 1- and 2D NMR data indicated the planar structure of **4** to be a methoxy derivative of didymellamide B (**3**) (Haga et al., 2013), and according to the observed HMBC correlation from H-26 to C-23 (δ_C: 158.5), its position determined to be at C-23 (Fig. 4). Similar to **2**, LC-MS analysis was carried out to confirm the presence of the compound in the EtOAc extract of the *Trochila* sp. BGP15P7IS3. The result indicated that this compound was produced by the fungus and was not an artefact of the isolation process (see Fig. S29). The NOESY spectrum showed NOE correlations between H-8 and H-18, H-14 and H-12, and H-8 and H-14. In addition, the experimentally measured ECD spectrum in MeOH showed also a good agreement with that of didymellamide B (**3**), as well as **1** (Fig. 5A), resulting in determining its absolute configuration as 8*R*,9*R*,12*R*,14*S*,17*R*.

Compound **5** was obtained as a white-brownish solid. Its molecular formula of $C_{24}H_{29}NO_4$ was determined on the basis of a HRESIMS data peak at *m/z* 396.2172 $[M + H]^+$ (calcd. for $C_{24}H_{30}NO_4^+$, 396.2169) and corresponding to 11 degrees of unsaturation. The ^{1}H NMR spectrum (Table 1) of **5** showed four aromatic protons [δ_H 7.28 (2H, m, H-21, 25), and 6.82 (2H, m, H-22, 24)]. In addition, two methyl groups [δ_H: 1.70 (3H, d, J = 6.1 Hz, H-18)] and [δ_H: 0.88 (3H, d, J = 6.7 Hz, H-19)], five olefinic protons [δ_H 7.48 (1H, brs, H-6), 5.50 (1H, m, H-14), 5.96 (1H, m,

Table 2
^{13}C (150 MHz) NMR Data of compounds **1**, **2**, **4**, **5**, and **8**.

Position	1 (DMSO-d_6)	2 (DMSO-d_6)	4 (DMSO-d_6)	5 (CD_3OD)	Position	8 ($CDCl_3$)
1	–		–	–	1	101.7
2	161.3	161.4	161.4	164.2	2 [b]	164.7
3	106.8	106.8	106.8	107.7	3	107.4
4	175.9	175.9	175.9	177.1	4 [b]	156.5
5	112.7	112.1	111.2	112.2	5	163.4
6	140.7	140.5	141.0	140.6	6	112.1
7	209.7	212.2	209.9	209.9	7	8.77
8	51.8	51.7	51.8	44.0	8	204.7
9	35.8	35.8	35.8	25.7	9	33.5
10	29.3	29.3	29.4	28.0	10	60.8
11	35.0	34.9	35.0	37.5	1′	101.7
12	32.5	32.4	32.5	34.5	2′ [b′]	164.7
13	41.3[a]	41.3[a,b]	41.3[a,b]	41.1	3′	107.4
14	41.3[a]	41.2[a,b]	41.3[a,b]	131.2	4′[b′]	156.5
15	130.3	130.2	130.3	133.1	5′	163.4
16	131.6	131.5	131.6	133.0	6′	112.1
17	30.6	30.5	30.6	127.4	7′	8.77
18	17.8	17.7	17.8	18.1	8′	204.7
19	22.4	22.3	22.4	20.0	9′	33.5
20	123.8	125.5	125.5	125.2	10′	60.8
21	120.0	119.7	130.2	131.4		
22	115.4	112.1	113.6	116.1		
23	144.9	147.1	158.5	158.3		
24	144.8	146.0	113.6	116.1		
25	116.6	116.5	130.2	131.4		
26	–	55.7	55.1	–		

[b,b′] interchangeable signals.
[a] overlapping signals; .

H-15), 6.00 (1H, m, H-16), and 5.55 (1H, m, H-17)], one methine group [δ_H: 1.50 (1H, m, H-12)] and five methylene groups [δ_H: 3.18 (2H, t, J = 7.4 Hz, H-8)], [δ_H: 1.66 (2H, m, H-9)], [δ_H: 1.42 (1H, m, H-10a) and 1.38 (1H, m, H-10b)], [δ_H: 1.38 (1H, m, H-11a) and 1.19 (1H, m, H-11b)], and [δ_H: 2.07 (1H, m, H-13a) and 1.90 (1H, m, H-13b)] were distinguished. The ^{13}C NMR (Table 2) and HSQC spectra revealed 24 carbon signals, including signals corresponding to the above structural units and additional signals for two carbonyls (δ_C: 164.2 and 209.9) and five quaternary carbons (δ_C: 107.7, 177.1, 112.2, 125.2, and 158.3). Comparison of the NMR spectroscopic data of **5** (Tables 1 and 2) with didymellamide B (**3**) reveals that both compounds possess a similar benzene ring and a 4-hydroxypyridone moiety. However, the decalin moiety in compound **3** was replaced by an unsaturated dodecane moiety in compound **5**, as indicated by the presence of five above-mentioned CH_2 groups, four unsaturated CH groups, and one aliphatic CH group, compared to three CH_2, two unsaturated CH, and five aliphatic CH groups in compounds **1**–**4**. This substitution was corroborated by the COSY correlations from H-9 to H-8, H-10a, and H-10b, from H-11b to H-10a, H-10b, and H-12, from H-12 to H-11, H-13, and H3-19, from H-13a to H-12, H-14, and H-15, from H-15 to H-14, and H-16, and from H-17 to H-16, and H-18, along with the HMBC correlations observed from H-19 to C-11, C-12, and C-13 (δ_C: 37.5, 34.5, and 41.1), from H-18 to C-17 and C-16 (δ_C: 127.4 and 133), and from H-8 to C-7 and C-9 (δ_C: 209.9 and 25.7) (Fig. 4). The configuration of the double bonds in C-14 to C-17 (δ_C: 131.2, 133.1, 133, and 127.4) was determined to be a *S*-trans configuration based on the similarity of ^{1}H and ^{13}C chemical shifts to those of ilicicolin H and epi-ilicicolin H biosynthesis precursors (*bis*-diene derivatives) (Zhang et al., 2019) and also lovastatin biosynthesis precursors such as (7*R*)-(*E*,*E*-10,10-Dimethoxy-7-methyldeca-2,4-diene (Witter and Vederas, 1996). Thus, the planar structure of **5** determined to be an undescribed pyridone-type alkaloid and was named didymellamide I (**5**) (Fig. 1). The absolute configuration of the chiral center at C-12 was deciphered as *R* by comparing the calculated and experimentally obtained ECD spectrum in MeOH (Fig. 5B).

Compound **8** was obtained as a white-brownish solid. Its molecular formula of $C_{20}H_{22}O_8$ was determined on the basis of a HRESIMS peak at *m/z* 391.1388 $[M + H]^+$ (calcd. for $C_{20}H_{23}O_8^+$, 391.1387) and corresponding to 10 degrees of unsaturation. The ^{1}H NMR spectrum (Table 1) of **8** in $CDCl_3$ showed two methyl groups [δ_H: 2.73 (3H, s, H-9, 9′)] and [δ_H: 2.14 (3H, s, H-7 and H-7′)], one methoxy group [δ_H: 3.55 (3H, s, H-10 and H-10′)]. The ^{13}C NMR (Table 2) and HSQC spectra revealed 10 carbon signals, including the signals corresponding to the structural units mentioned above, and additional signals for a carbonyl group (δ_C: 204.7) and six quaternary carbons (δ_C: 164.7, 107.4, 156.5, 163.4, 112.1, and 101.7). Analyzing the 1- and 2D NMR data of **8**, along with its calculated molecular formula suggested that it possesses a highly symmetric structure. The HMBC spectrum for **8** revealed correlations from H-9 to C-8 and C-3 (δ_C: 204.7 and 107.4), confirming the position of acetyl moiety; from H-10 to C-5 (δ_C: 163.4), and from H-7 to C-6, C-5, and C-1 (δ_C: 112.1, 163.4, and 101.7), determining the position of methoxy and methyl group, respectively (Fig. 4). The remaining ^{13}C NMR signals were attributable to two sp^2 quaternary carbons, indicating the presence of two hydroxyl groups, the position of which could be established through the long-range correlations from H-7 to C-2 and C-4 (δ_C: 164.7 and 156.5). Furthermore, taking into account the degrees of unsaturation and the lack of correlation from or to C-1, this carbon could be identified as the center of symmetry. Considering all the above information, the structure of compound **8** was identified as a previously undescribed biphenyl derivative and named as trochinol A (Fig. 1). To determine whether it is optically active due to the presence of the chirality axis (C1–C1′), the optical rotation and ECD spectrum were measured. However, no optical activity was observed, suggesting the presence of a racemic mixture.

Besides the undescribed compounds reported, compound **7** was identified as didymellamide C, however, its absolute configuration was not fully deciphered in the previous reports (Haga et al., 2013). To this end, the relative configuration of **7** at the decalin ring was first determined using a NOESY spectrum (Fig. S54), which was similar to the compound **1** (Fig. 6A). Subsequently, ECD calculations were performed for two possible epimers of **7** (8*R*,9*R*,12*R*,14*S*,17*R*,20*R* and 8*R*,9*R*,12*R*,14*S*,17*R*,20*S*), since only the relative configuration at C-22 remained ambiguous. Comparison of the calculated and experimental ECD spectra obtained in MeOH led to the determination of the absolute configuration of **7** as 8*R*,9*R*,12*R*,14*S*,17*R*,20*R* (Fig. 6A). Compounds **9** and **10** were

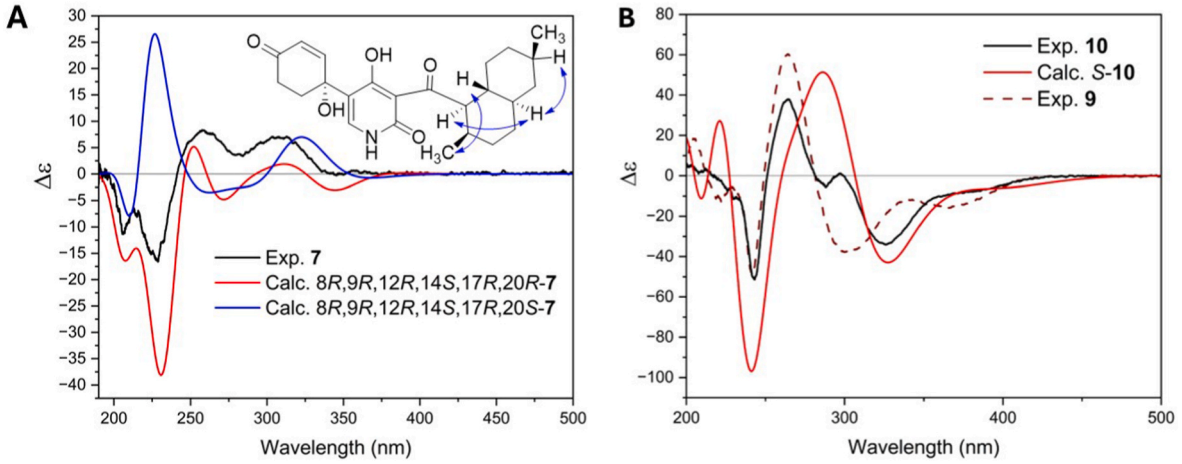

Fig. 6. A) NOESY correlations of **7**, and experimental versus calculated ECD spectra for two epimers of **7** in MeOH, B) experimental ECD spectra of **9** and **10** and calculated ECD spectrum of **10** in acetonitrile.

identified as isousnic acid and usnic acid derivatives, respectively, according to the obtained NMR data (see Figs. S55–58 and Table S2) and comparison to the literature data (Bui et al., 2021; Rashid et al., 1999). To determine their absolute configuration, their ECD spectrum was measured in acetonitrile and compared with the simulated ECD spectrum for **10**, as an example (Fig. 6B). The results show a great match with the calculated ECD spectrum, corresponding to an *S* configuration at the corresponding stereocenter. To the best of our knowledge, this is the first report of *S*-usnic acid and *S*-isousnic acid from endophytic resources. The *S* stereoisomer is quite rare in nature and has only been reported from lichen species belonging to a few genera including *Alectoria* (Parmeliaceae) and *Cladonia* (Cladoniaceae) (Xu et al., 2022; Bézivin et al., 2004).

Han et al. (2017) and Wang et al. (2015) have previously proposed two possible biogenesis pathways for pyridone-type alkaloids, starting from one L-tyrosine, one acetyl-CoA, and six malonyl-CoA units, in both of which, cyclization through Diels-Alder reaction to form the decalin ring takes place prior to intramolecular Claisen cyclization to form the tetramic acid core c (Fig. 7). However, another potential biogenetic pathway for the pyridone-type alkaloids is postulated here (Fig. 7), since in this study the isolation of compound **5** can serve as a likely precursor for biosynthesis and identified another potential derivative of **5** via FBMN (Fig. 7). The linear polyketide precursor initially condenses with an activated L-tyrosine to form the intermediate **a**. The intermediate **a**n undergoes intramolecular Claisen cyclization to yield tetramic acid core (intermediate **b**), which in turn subjects to ring expansion through series of hydroxylation, dehydration, and rearrangement to form pyridone core (intermedia **c**). Conversely, the polyketide chain reduces to form intermediate **d** and subsequently **e**, which in turn undergoes a Diels-Alder reaction to generate decalin ring and intermediate **f** (compound **3**). Through series of transformations, including reduction, and hydroxylation, and O-methylation, respective compounds are produced.

2.4. Antimicrobial activity of the compounds isolated

The compounds isolated were evaluated for their bioactivity against

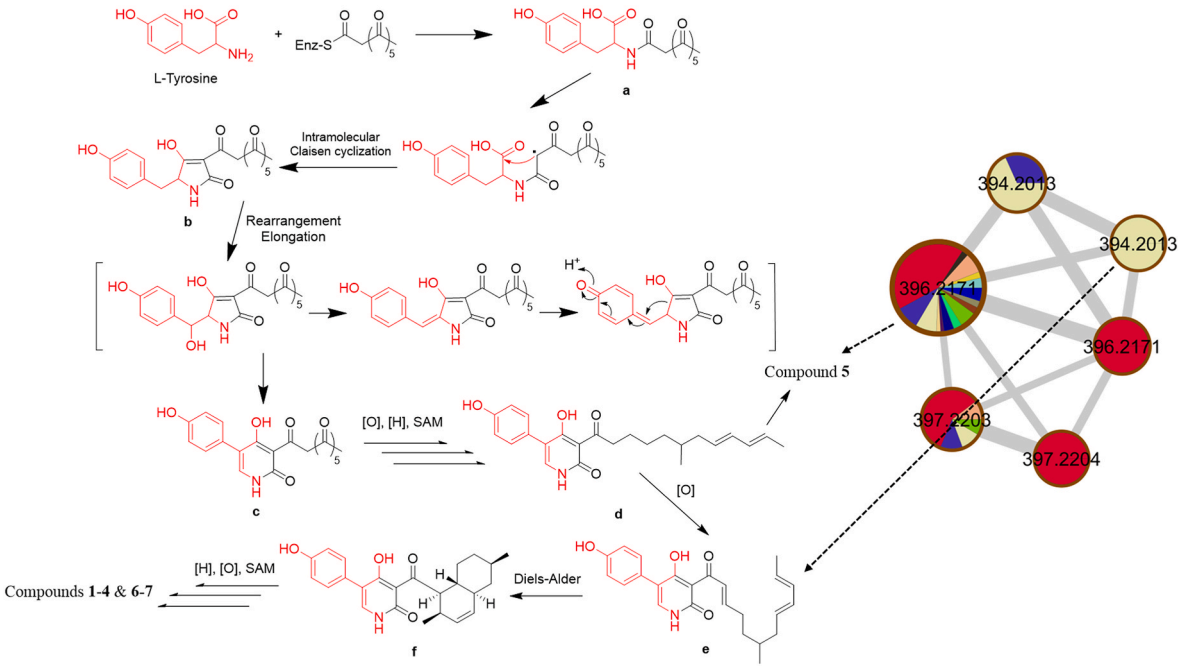

Fig. 7. Putative biosynthesis pathway of **1**–**7**.

B. cinerea, a human protozoal parasite *T. vaginalis*, and additional four human fungal pathogens, *A. fumigatus*, *A. flavus*, *C. albicans*, *C. neoformans*. As shown in Fig. 8A, the results obtained revealed compound **6** to inhibit *B. cinerea* growth with a MIC value of 0.78 μg/mL, which was comparable to hygromycin B, the positive control used in this study (MIC = 0.39 μg/mL) (Fig. 8A and Table 3). Furthermore, compounds **6** and **9** illustrated a concentration-dependent growth inhibition of human sextually transmitted parasite, *T. vaginalis* (Fig. 8B and C, respectively). Evaluation of antifungal activities of the compounds isolated against four human fungal pathogens after 48 h incubation indicated compound **6** with MIC values of 6.25, 25, 3.12, and 3.12 μg/mL to be the most active substance against *A. fumigatus*, *A. flavus*, *C. albicans*, *C. neoformans*, respectively. Additionally, compound **3** displayed antifungal activity only against *C. neoformans* with MIC value of 12.5 μg/mL (Fig. 9, Table 3).

3. Conclusions

In conclusion, a total of eleven compounds were isolated from the rice culture of *Trochila* sp. BGP15P7IS3, an endophytic fungus of *L. carniolicum*. Compounds **1**, **2**, **4**, **5**, and **8** were identified as undescribed natural products. *S*-isousnic acid (**9**) and *S*-usnic acid (**10**) were identified as rare stereoisomers and previously unreported from an endophytic fungus. Evaluation of the bioactivity of the compounds against several human and plant pathogens resulted in identification of compound **6** as the most active compound against *B. cinerea*, *T. vaginalis*, *A. fumigatus*, *A. flavus*, *C. albicans*, and *C. neoformans*. Compound **3** conversely could inhibit only *C. neoformans*.

In this study, implementing molecular networking of the GNPS platform provided valuable information on the chemical space of the fungus, *Trochila* sp. BGP15P7IS3 and its genus for the first time. This approach enabled the dereplication of several pyridone alkaloid and dihydobenzofuran derivatives, as well as the identification of previously unreported substances for targeted isolation. As demonstrated, and in line with previous reports on antimicrobial activity of this class of compounds, their occurrence in endophytes may enhance the ability of plants to withstand biotic stresses imposed by phytopathogens such as *Botrytis* species. Furthermore, two rare isomers of usnic acid and isousnic acid, which were isolated in this work, have previously been reported to promote plant growth and exhibit promising antimicrobial activities against various plant pathogens. The biosynthesis of these two compounds, together with other potential derivatives in relatively high amounts in this fungus, along with the occurrence of bioactive pyridone-type alkaloids indicates its potential role as a biocontrol agent. Nonetheless, further studies are required to investigate this hypothesis through greenhouse and field experiments.

4. Experimental section

4.1. General experimental procedures

Optical rotations measurements were carried out using a Jasco P-2000 polarimeter (Jasco, Japan), in a 10.0 cm length cell, using MeOH or $CHCl_3$. IR spectra were recorded on an Alpha-II FTIR spectrometer (Bruker). UV and ECD spectra were measured on a J-1500 spectropolarimeter (JASCO, Japan). NMR spectra were acquired on an Avance II (600 MHz, Bruker, USA) and residual solvent peaks were utilized for internal referencing of the chemical shifts. HRESIMS

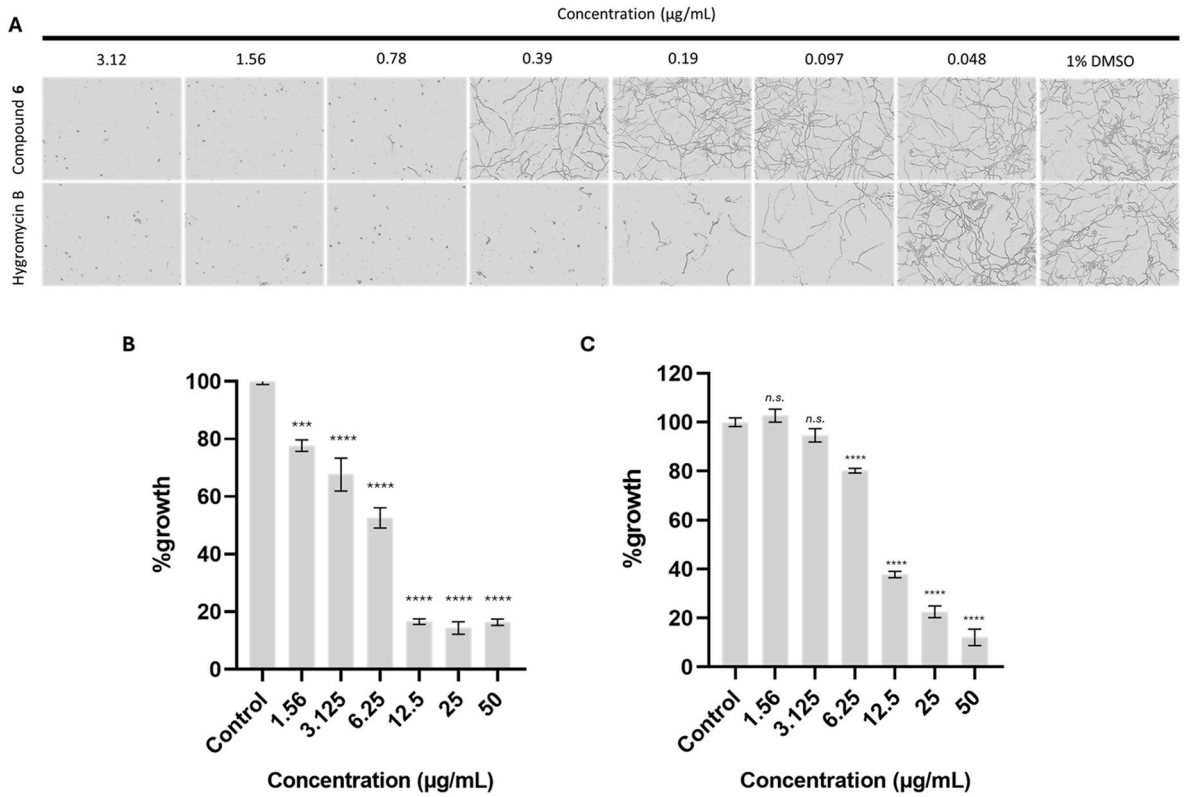

Fig. 8. A) MIC values of compound **6** against *B. cinerea*. The spores (10^4/well) were incubated for 48 h with various concentrations of **6**. The images were taken by Incucyte 3.0 at 50× magnification. All experiments were performed in triplicate (n = 3) and representative images from one replicate are shown. Hygromycin B was utilized as the positive control with MIC value of 0.39 μg/mL; B and C) Concentration-dependent growth inhibition effect of compound **6** (8-B) and **9** (8-C) against human sextually transmitted parasite, *T. vaginalis*. The experiments were conducted in triplicate (n = 3) and the results are presented as %growth ± SEM. Statistical significance was determined using one-way ANOVA followed by Dunnett's multiple comparisons test, comparing each concentration to the control group. $p < 0.05$ was considered statistically significant (***$p = 0.0002$, ****$p < 0.0001$). Metronidazole with EC_{50} value of 3 μg/mL was utilized as the positive control in this study (data not shown).

Table 3
Minimum inhibitory concentration (MIC) values of the isolated compounds against *B. cinerea* and four human fungal pathogens.

MIC (μg/mL) ranges					
Compounds	*B. cinerea*	*A. fumigatus*	*A. flavus*	*C. albicans*	*C. neoformans*
3	>50	>50	>50	>50	12.5
6	0.78	6.25	25	3.12	3.12
Hygromycin B	0.39	–	–	–	–
Voriconazole	–	0.25	1	0.02	0.5

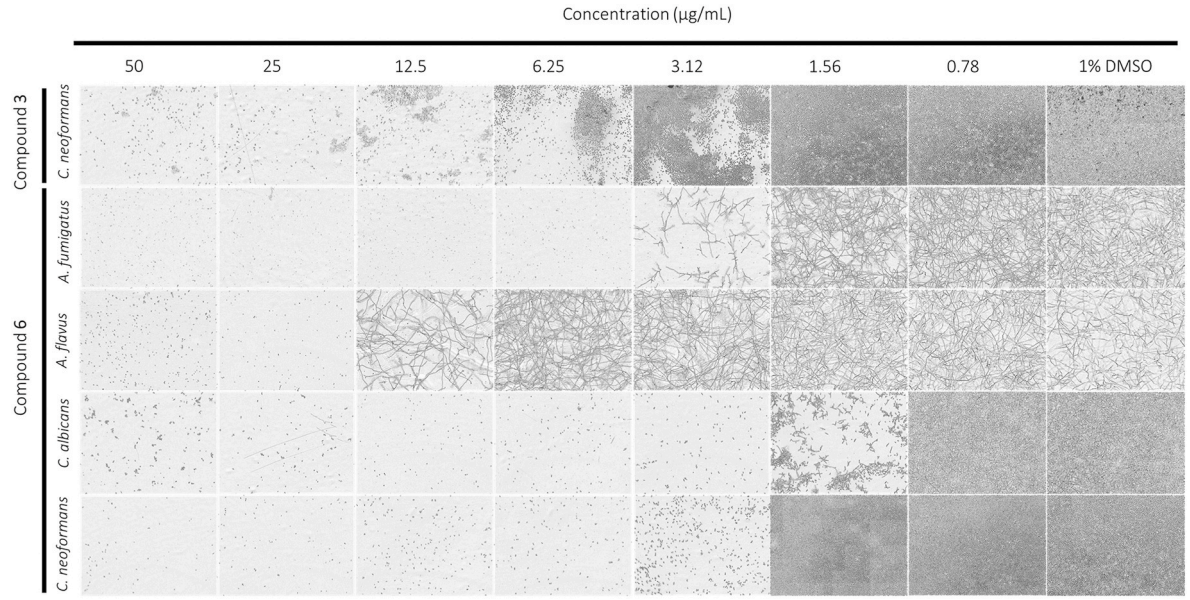

Fig. 9. Antifungal activity of compounds **3** and **6** against four human fungal pathogens. The concentrations are illustrated as μg/mL. The spores (10^4/well) were incubated for 48 h with various concentrations of **3** and **6**. Microscopic images were taken after 48 h using the IncuCyte S3 Live-Cell Analysis System. All experiments were performed in triplicate (n = 3) and representative images from one replicate are shown. Voriconazole was used as the positive control for all strains with the following MIC values: 0.25 μg/mL (*A. fumigatus*), 1 μg/mL (*A. flavus*), 0.02 μg/mL (*C. albicans*), and 0.5 μg/mL (*C. neoformans*).

analyses were carried out using Exploris-120 Orbitrap mass spectrometer coupled to a Vanquish UPLC system, equipped with a Vanquish variable wavelength detector (Thermo Fischer Scientific, MA, USA). Fractionation of the fungal extract was carried out on a Reveleris® system (Buchi, Switzerland) using a silica gel cartridge. For conventional column chromatography silica gel or Sephadex LH-20 (Sigma-Aldrich, USA) were utilized as the stationary phase. Analytical HPLC was performed on an Agilent 1200 system equipped with a degasser, autosampler, column compartment, and a PDA detector, using a Phenomenex Synergi MAX-RP 250 × 10 mm, 4 μm, 80 Å column. TLC analysis of the fractions was performed on precoated silica gel 60 F_{254} (0.25 mm, Merck) plates, and spots were visualized using an anisaldehyde spray reagent and heat. All solvents required for extraction and isolation were purchased from VWR (Austria). Ultrapure water was produced by a Sartorius arium 611 UV system (Germany).

4.2. Fungal material

4.2.1. Isolation and identification

Fungal species were isolated from the leaves of *L. carniolicum*, collected in the botanical garden in Mt. Patscherkoferl (1700 m a.s.l), Innsbruck, Austria, after surface sterilization. Briefly, leaf surfaces were treated in the sequence 70 % ethanol, 2 % sodium hypochlorite solution, 70 % ethanol, and ultimately sterilized water. Sterilized leaves were cut into pieces, placed on a Malt Extract Agar (MEA) plate and, alternatively, Wickerham medium plates and incubated for 4 weeks at 25 °C in the dark. Pure cultures of *Trochila* sp. BGP15P7IS3 have been deposited at the culture collection of the Department for Microbiology, University Innsbruck (Herbarium No. IBF20210185). Microscopic data was documented with a Nikon camera DSFi1 in combination with the computer program NIS-Elements D 3.0. Microscopical examinations showed that the pure culture isolate of *Trochila* sp. BGP15P7IS3 did not produce any reproductive structures. For identification of the fungus, genomic DNA (gDNA) was extracted from mycelium harvested from Wickerham medium. The identification was based on a multigene approach including the rDNA region LSU, ITS, SSU, and the RPB2 region. The internal transcribed spacer (ITS) regions of the ribosomal DNA were amplified using the primer pair ITS-1F (5′-CTTGGTCATTTAGAGGAAGTAA-3′) and ITS-4 5′-TCCTCCGCTTATTGATATGC-3′). Sequencing of the PCR products was performed by Microsynth (Microsynth AG, Switzerland). Sequences are available from GenBank under the respective accession numbers (see Table S1). BLAST-searches were conducted against UNITE (http://unite.et.ee) and GenBank (http://ncbi.nlm.nih.gov/). Highly similar sequences were downloaded from UNITE. Sequences of type material were also included in the analysis (see Table S1). The phylogenetic analysis of rDNA ITS sequences involved 23 nucleotide sequences. The outgroup was selected based on published sister group relationships (Gómez-Zapata et al., 2021). The concatenated rDNA analysis included 5 sequences, the analysis of RPB2 7 sequences. Sequences were automatically aligned in MUSCLE (Edgar, 2004) and analyzed with RAxML on T-REX (Alix et al., 2012). Evolutionary history was inferred by Maximum Likelihood with the GTR model with discrete Gamma distribution. It was run with Rapid Bootstrapping, searching for the best scoring ML tree, and 500 replicates. Additionally, branch robustness was tested with Bayesian Inference in MrBayes v. 3.2.6 (Huelsenbeck and Ronquist, 2001). GTR was used as substitution model,

and a gamma distribution of rate variation across sites was chosen. For prior probability settings defaults were kept. For the Markov Chain Monte Carlo (MCMC) analyses, four chains were run for 2 M generations, with trees being sampled every 1000 generations. The analysis was stopped as the convergence diagnostic (average standard deviation of split frequencies) was below 0.05 after 10 M generations. From the sampled trees, 25 % were discarded as burn-in before summary statistics were calculated (using sump and sumt commands). Diagnostic plots, as well as the convergence diagnostics EES (Estimated Sample Size; min ESS around 10 K) and PSRF (Potential Scale Reduction Factor; 1.000 for all parameters), indicated stationarity.

4.2.2. Upscaling and extraction of fungal material

Trochila sp. BGP15P7IS3 was cultured in MEA plates and were inoculated on rice medium (100 g rice+110 mL H_2O) in 10 × 1L Erlenmeyer flasks. The flasks were kept at 25 °C and in dark conditions for 60 days to reach the maximum growth. The fungal materials were combined and extracted eight times with EtOAc (8 × 800 mL) using ultrasonic bath (20 min). Obtained extract was evaporated on a rotary evaporator to yield 2.5 g of a crude extract.

4.3. Extraction and isolation

The obtained crude extract (2.5 g) was subsequently fractionated on a silica gel column using an MPLC system using gradients of petroleum ether-DCM (100:0 to 0:100) and DCM-MeOH (100:0 to 0:100) to yield 40 subfractions. Fractions 4 and 8, eluted from petroleum ether-DCM at approximately 45:55 and 40:60, respectively, were obtained as pure crystalline substances, yielding compounds **10** (29 mg) and **9** (12.1 mg). F12 (55 mg) was separated on a silica gel column (Ø: 0.5 mm, L: 30 mm) using DCM-MeOH (85:15) to afford compound **8** (3.5 mg). Fraction 15 (76.1 mg) was further separated on a Sephadex LH-20 column (Ø: 25 mm, L: 870 mm) using DCM-Acetone (85:15) to yield further 7 subfractions. F15_5 (9.2 mg) was purified on a silica gel column (Ø: 10 mm, L: 31 mm) with DCM-MeOH (99.3:0.8) as the mobile phase to yield compound **4** (4.9 mg). Fraction 18 (233.2 mg) was subjected to chromatography on an LH-20 column (Ø: 25 mm, L: 870 mm) using DCM-Acetone (85:15) as the mobile phase to yield compound **6** (17.6 mg) and compound **3** (29.5 mg). Subsequently its subfraction F18_25 (17.5 mg) was subjected to a silica gel column (Ø: 35 mm, L: 900 mm) using isocratic elution with DCM-MeOH (98:2) as the mobile phase, yielding **2** (1.2 mg) and **7** (6.6 mg). Additionally, subfraction F18_39 (6 mg) was purified on a silica gel column (Ø: 0.5 mm, L: 30 mm) using DCM-MeOH (85:15) to afford compound **5** (1.5 mg). F20 (22.1 mg) was subjected to chromatography on a Sephadex LH-20 column (Ø: 35 mm, L: 900 mm) using MeOH as the mobile phase to give compound **1** (3.4 mg). F27-29 were combined (132 mg) and were purified on a Sephadex LH-20 column (Ø: 35 mm, L: 900 mm) using MeOH as the mobile phase to give compound **11** (20 mg).

4.3.1.

24-hydroxy didymellamide B (**1**): white-brownish solid; $[\alpha]_D^{25}$ −30.2 (*c* 0.05, MeOH); UV (MeOH) λ_{max} (log ε) 211 (3.02), 254 (2.73), 309 (2.26) nm; ECD (c = 1.33 mg/mL) MeOH) λ_{max} (mdeg) 209.5 (−7.64), 248 (−3.80), 317.1 (+2.59); UV λ_{max} (log ε) 198 (1.72), 250 (0.88), 346 (0.296); IR (ATR) ν_{max}: 2916, 1648, 1604, 1520, 1456, 1209, 1024 cm^{-1}; ^1H NMR (600 MHz, DMSO-d_6) and ^{13}C NMR (150 MHz, DMSO-d_6) data (Table 1, Table 2); HRESIMS *m/z*: 410.1959 $[M + H]^+$ (calcd. for $C_{24}H_{28}NO_5^+$, 410.1962).

4.3.2.

23-methoxy-24-hydroxy didymellamide B (**2**): white-brownish solid; $[\alpha]_D^{25}$ −64.6 (*c* 0.05, MeOH); UV (MeOH) λ_{max} (log ε) 198 (4.15), 249 (3.78), 285 (3.66), 348 (3.22) nm; ECD (c = 0.1 mg/mL MeOH) λ_{max} (mdeg) 206.6 (−6.88), 242.8 (−3.47), 314 (+1.99); IR (ATR) ν_{max}: 2917, 1649, 1603, 1513, 1455, 1211 cm^{-1}; ^1H NMR (600 MHz, DMSO-d_6) and ^{13}C NMR (150 MHz, DMSO-d_6) data (Table 1, Table 2); HRESIMS *m/z*: 424.2119 $[M + H]^+$ (calcd. for $C_{25}H_{30}NO_5^+$, 424.2118).

4.3.3.

Methoxydidymellamide B (**4**): white-brownish solid, $[\alpha]_D^{25}$ −145.8 (*c* 0.068, MeOH); UV (MeOH) λ_{max} (log ε) 191.5 (4.21), 246.6 (3.86), 349.7 (3.33) nm; ECD (c = 0.13 mg/mL, MeOH) λ_{max} (mdeg) 205.4 (−13.4), 246.5 (−8.4), 276.7 (+1.26), 319 (+3.17); IR (ATR) ν_{max}: 2908,1649,1600, 1451, 1247, 1034, 831 cm^{-1}; ^1H NMR (600 MHz, DMSO-d_6) and ^{13}C NMR (150 MHz, DMSO-d_6) data (Table 1, Table 2); HRESIMS *m/z*: 408.2169 $[M + H]^+$ (calcd. for $C_{25}H_{30}NO_4^+$, 408.2169).

4.3.4.

Didymellamide J (**5**): white-brownish solid, $[\alpha]_D^{25}$ +36.1 (*c* 0.19, MeOH); UV (MeOH) λ_{max} (log ε) 193 (4.35), 230 (4.15), 348 (3.49) nm; ECD (c = 0.084 mg/mL, MeOH) λ_{max} (mdeg) 203.2 (−4.147), 308.8 (+0.75), 353.2 (−0.35); IR (ATR) ν_{max}: 2.5, 1650, 1609, 1456, 1269, 835 cm^{-1}; ^1H NMR (600 MHz, CD_3OD) and ^{13}C NMR (150 MHz, CD_3OD) data (Table 1, Table 2); HRESIMS *m/z*: 396.2171 $[M + H]^+$ (calcd. for $C_{24}H_{30}NO_4^+$, 396.2169).

4.3.5.

Trochinol A (**8**): white-brownish solid, UV (MeOH) λ_{max} (log ε) 224 (4.05), 280 (4.03), 341 (3.41) nm; IR (ATR) ν_{max}: 2931, 1586, 1411, 1368, 1279, 1106, 584 cm^{-1}; ^1H NMR (600 MHz, $CDCl_3$) and ^{13}C NMR (150 MHz, $CDCl_3$) data (Table 1, Table 2); HRESIMS *m/z*: 391.1387 $[M + H]^+$ (calcd. for $C_{20}H_{22}O_8^+$, 391.1387).

4.4. UHPLC-HR-MS/MS analysis

Subfractions obtained in sufficient amounts (>15 mg) from the EtOAc extract of *Trochila* sp. BGP15P7IS3 were analyzed by a Vanquish UPLC system coupled with an Exploris-120 mass spectrometer (Thermo Scientific, USA). The separation was carried out on an Accucore C18, 150 × 2.1 mm, 2.6 μm column using the following gradient and parameters: mobile Phase: A = H_2O+0.1 % FA, B=CH_3CN+0.1 % FA, gradient: t = 0 Min: 5 % B; t = 0–20 Min: linear increase to 99 % B; t = 20–27 Min: hold at 99 % B; temperature: 35 °C; flow rate: 0.4 mL/min, injection volume: 1 μL (Conc.: 3 mg/mL). The instrument was controlled by Thermo Scientific Xcalibur 4.4 software. The MS analysis was conducted in positive mode using the following parameters for MS^1: Spray voltage: 3200 V, Sheath gas (N2): 45 arbitrary unit, auxiliary gas (N2): 17 arbitrary units, ion transfer tube temperature: 350 °C, vaporizer temperature: 400 °C., RF Lense (%): 70, microscans: 1. MS^1 data were recorded in a mass range of 150–1500 *m/z* with a resolution of 60000 FWHM, and in centroid mode. Data dependent experiments (dd-MS^2) were carried out for top 3 ions, resolution was set to 15000 FWHM, for precursor fragmentation in the HCD mode, a normalized collision energy (stepped) of 15, 30 and 45 % was utilized and the data was recorded in centroid mode. The following filters were included in the measurements: intensity threshold (1.5 E^5), dynamic exclusion (exclude after 1 time, duration: 3, mass tolerance ±10 ppm), apex detection (30 %), isotopic exclusion filter (assigned), charge state (1), as well as a targeted mass exclusion list.

4.5. MS data analysis, Feature-Based Molecular Networking, SIRIUS

Raw MS/MS data of the fractions with sufficient amounts were processed via MZmine 4.6 software (Pluskal et al., 2010). Aligned feature list were submitted to the GNPS Web platform (http://gnps.ucsd.edu) for generation of the Feature-Based Molecular Network. The following parameters were utilized: precursor mass tolerance, 0.02 Da; MS/MS fragment ion tolerance, 0.02 Da; minimum cosine score, 0.7; minimum matched fragment ions, 5; minimum cluster size, 2; network

TopK, 10. The generated molecular network was further visualized and analyzed using Cytoscape 3.8.2 (Shannon et al., 2003). The job can be accessed from the GNPS platform using the following link: https://gnps.ucsd.edu/ProteoSAFe/status.jsp?task=3dae1a6830b64150baa75a7ae558caab. To obtain information on the structural classes presented in the extract, the aligned feature list was submitted to SIRIUS. The data obtained were filtered using following criteria: min_ZodiacScore = 0.9, min_ConfidenceScore = 0.1, min_class_confidence = 0.8. The filtered features and the respective annotations were summarized in a.tsv file and used for visualization of compound classes using a python script (see Fig. S2).

4.6. ECD calculation

Conformational analysis of the compounds was carried out using MacroModel 9.1 (Schrödinger. LLC, New York, NY, USA) and OPLS-3 as the force field, and in the gas phase. Geometrical optimization and energy calculations of conformers occurring in the energy window of 5 kcal mol^{-1} were carried out at DFT/6-31G(d,p) level in gas phase using Gaussian 16 (Frisch et al., 2016). No imaginary frequencies were observed. Subsequently, the conformers with population over 3 % (refer to the Supplementary Material) were subjected to ECD calculation at TD-DFT/B3LYP-6-31G(d,p)/CPCM in methanol or acetonitrile. ECD spectra obtained (with a half-band of 0.25 eV) were Boltzmann-averaged and further compared with experimental spectra obtained in methanol or acetonitrile using SpecDis v. 1.71 (Bruhn et al., 2017). No UV shift correction was required.

4.7. Antimicrobial activity assays

4.7.1. Antifungal susceptibility testing and minimum inhibitory concentration (MIC) evaluation against fungal pathogens

Aspergilli conidia and yeast cells were amplified on Sabouraud dextrose (SAB, Sigma-Aldrich Corp., St. Louis, MI, USA) medium with incubation at 37 °C for 3 and 2 days, respectively. For the screening of extracts, fractions, and compounds for potential antifungal activity against *A. fumigatus* (A1160P+) (Fraczek et al., 2013), *A. flavus* (ATCC, 204304) (Espinel-Ingroff et al., 1997), *C. albicans* (SN152) (Homann et al., 2009)and *C. neoformans* (H99) (Jung et al., 2015), RPMI-1640 containing 2 % glucose was used. Generally, assays were perfo = rmed in 96-well plates with an inoculum of 1×10^5/mL conidia or yeast cells in a final volume of 200 µl at 37 °C for up to 48 h. Initial screenings for cell extracts with antifungal activity were performed with a final concentration of 100 µg/mL of each extract. For extracts with antifungal activity, broth microdilution (2-fold) MICs were determined. MIC values were evaluated by eye. Microscopic images were taken after 24 and 48 h using the IncuCyte S3 Live-Cell Analysis System (Essen Bioscience Inc., Ann Arbor, MI, USA) as previously described (Kühbacher et al., 2024). All experiments were performed in triplicate (n = 3) and representative images from one replicate are shown.

4.7.2. Antifungal assay against Botrytis cinerea

B. cinerea (B05.10) was cultivated on Potato Dextrose Agar (PDA) medium and incubated at 25 °C for 10 days. The conidia were harvested with spore buffers and counted. The bioassay was performed in 96-well plates using Potato Dextrose Medium (PDB), containing an inoculum of 1×10^5/mL spores in a final volume of 100 µL at 25 °C. The extracts and fractions were evaluated at single concentration of 100 and 50 µg/mL, respectively and for the pure metabolites, broth microdilution (2-fold) MICs were determined. MIC values were evaluated by eye and microscopic images were taken after 24 and 48 h using the IncuCyte S3 Live-Cell Analysis System (Essen Bioscience Inc., Ann Arbor, MI, USA). All experiments were performed in triplicate (n = 3) and representative images from one replicate are shown.

4.7.3. Antiparasitic activity of assessment against Trichomonas vaginalis

Trichomonas vaginalis strain G3 (ATCC PRA-98) was cultivated in TYM medium. After the cells reached their maximum growth (typically 48 h), the protozoites were counted and seeded in 96 well plate, containing 60×10^4 protozoa per well in final of volume of 200 µL media. Concomitantly the cells were treated with various concentrations of extracts, fractions, and/or pure compounds and the plates were placed inside a sealed box along with a CO_2 generating Sachet (Fischer Scientific, USA) to make an anaerobic environment for its growth. After 48h incubation at 37 °C, the plates were evaluated by microscope and turbidity of the wells were measured at OD_{600} to evaluate the concentration-dependent growth inhibitory effects of the compounds isolated. The experiments were conducted in triplicate (n = 3) and the results were expressed as %growth ± SEM. Statistical analysis was carried out using one-way ANOVA followed by Dunnett's multiple comparisons test, where each drug concentration was compared to the control group. A *p*-value of less than 0.05 was considered statistically significant. Graphs were generated using GraphPad Prism v. 9.0.

CRediT authorship contribution statement

Mostafa Alilou: Writing – review & editing, Writing – original draft, Visualization, Validation, Supervision, Resources, Project administration, Methodology, Investigation, Funding acquisition, Formal analysis, Data curation, Conceptualization. **Yun Liu:** Methodology, Investigation. **Magdalena Steixner:** Methodology, Investigation. **Isidor Happacher:** Writing – review & editing, Methodology, Investigation. **Sigrid Beate Abt:** Methodology, Investigation. **Ursula Fürnkranz:** Writing – review & editing, Formal analysis. **Fabio Gsaller:** Writing – review & editing, Resources, Methodology. **Ursula Peintner:** Writing – review & editing, Formal analysis, Data curation. **Hubertus Haas:** Writing – review & editing, Resources, Formal analysis.

Declaration of competing interest

The authors declare that they have no known competing financial interests or personal relationships that could have appeared to influence the work reported in this paper.

Acknowledgements

The authors are grateful for the financial support provided in part by the Austrian Science Fund (FWF, No. P37001B) and Forschungszentrum Berglandwirtschaft at the University of Innsbruck. Furthermore, the authors acknowledge in part the HPC facilities at the University of Innsbruck, for providing computational resources and Dr. Iwona Lesiak-Markowicz from the ISPTM at the Medical University of Vienna for additional help in handling *T. vaginalis*. Moreover, special thanks go to Petra Merschak at the institute of molecular biology at the Medical University of Innsbruck (MUI) for her help with performing assays on human fungal pathogens.

Appendix B. Supplementary data

Supplementary data to this article can be found online at https://doi.org/10.1016/j.phytochem.2025.114684.

Data availability

Data will be made available on request.

References

Alix, B., Boubacar, D.A., Vladimir, M., 2012. T-REX: a web server for inferring, validating and visualizing phylogenetic trees and networks. Nucleic Acids Res. 40, W573–W579. https://doi.org/10.1093/nar/gks485.

Aslam, B., Asghar, R., Muzammil, S., Shafique, M., Siddique, A.B., Khurshid, M., Ijaz, M., Rasool, M.H., Chaudhry, T.H., Aamir, A., Baloch, Z., 2024. AMR and sustainable development goals: at a crossroads. Glob. Health 20, 73. https://doi.org/10.1186/s12992-024-01046-8.

Bézivin, C., Tomasi, S., Rouaud, I., Delcros, J.G., Boustie, J., 2004. Cytotoxic activity of compounds from the lichen: *cladonia convoluta*. Planta Med. 70, 874–877. https://doi.org/10.1055/s-2004-827240.

Bruhn, T., Schaumloffel, A., Hemberger, Y., Pecitelli, G., 2017. Specdis Version 1.71; Berlin, Germany.

Bui, V.M., Huynh, B.L.C., Pham, N.K.T., Nguyen, T.A.T., Nguyen, T.T.T., Nguyen, K.P.P., Nguyen, T.P., 2021. Usneaceratins A and B, two new specialized metabolites from the lichen *Usnea ceratina*. Nat. Prod. Res. 36, 3945–3950. https://doi.org/10.1080/14786419.2021.1901288.

Dührkop, K., Fleischauer, M., Ludwig, M., Aksenov, A.A., Melnik, A.V., Meusel, M., Dorrestein, P.C., Rousu, J., Böcker, S., 2019. Sirius 4: a rapid tool for turning tandem mass spectra into metabolite structure information. Nat. Methods 16, 299–302. https://doi.org/10.1038/s41592-019-0344-8.

Edgar, R.C., 2004. MUSCLE: a multiple sequence alignment method with reduced time and space complexity. BMC Bioinf. 5, 113. https://doi.org/10.1186/1471-2105-5-113.

Espinel-Ingroff, A., Bartlett, M., Bowden, R., Chin, N.X., Cooper, C., Fothergill, A., McGinnis, M.R., Menezes, P., Messer, S.A., Nelson, P.W., Odds, F.C., Pasarell, L., Peter, J., Pfaller, M.A., Rex, J.H., Rinaldi, M.G., Shankland, G.S., Walsh, T.J., Weitzman, I., 1997. Multicenter evaluation of proposed standardized procedure for antifungal susceptibility testing of filamentous fungi. J. Clin. Microbiol. 35, 139–143. https://doi.org/10.1128/jcm.35.1.139-143.1997.

Fadiji, A.E., Babalola, O.O., 2020. Elucidating mechanisms of endophytes used in plant protection and other bioactivities with multifunctional prospects. Front. Bioeng. Biotechnol. 8, 467. https://doi.org/10.3389/fbioe.2020.00467.

Feng, P., Shang, Y., Cen, K., Wang, C., 2015. Fungal biosynthesis of the bibenzoquinone oosporein to evade insect immunity. Proc. Natl. Acad. Sci. USA 112, 11365. https://doi.org/10.1073/pnas.1503200112.

Fraczek, M.G., Bromley, M., Buied, A., Moore, C.B., Rajendran, R., Rautemaa, R., Ramage, G., Denning, D.W., Bowyer, P., 2013. The cdr1B efflux transporter is associated with non-cyp51a-mediated itraconazole resistance in *Aspergillus fumigatus*. J. Antimicrob. Chemoth. 68, 1486–1496. https://doi.org/10.1093/jac/dkt075.

Frisch, M.J., Trucks, G.W., Schlegel, H.B., Scuseria, G.E., Robb, M.A., Cheeseman, J.R., Scalmani, G., Barone, V., Petersson, G.A., Nakatsuji, H., Li, X., Caricato, M., Marenich, A., Bloino, J., Janesko, B.G., Gomperts, R., Mennucci, B., Hratchian, H.P., Ortiz, J.V., Izmaylov, A.F., Sonnenberg, J.L., Williams-Young, D., Ding, F., Lipparini, F., Egidi, F., Goings, J., Peng, B., Petrone, A., Henderson, T., Ranasinghe, D., Zakrzewski, V.G., Gao, J., Rega, N., Zheng, G., Liang, W., Hada, M., Ehara, M., Toyota, K., Fukuda, R., Hasegawa, J., Ishida, M., Nakajima, T., Honda, Y., Kitao, O., Nakai, H., Vreven, T., Throssell, K., Montgomery Jr., J.A., Peralta, J.E., Ogliaro, F., Bearpark, M., Heyd, J.J., Brothers, E., Kudin, K.N., Staroverov, V.N., Keith, T., Kobayashi, R., Normand, J., Raghavachari, K., Rendell, A., Burant, J.C., Iyengar, S.S., Tomasi, J., Cossi, M., Millam, J.M., Klene, M., Adamo, C., Cammi, R., Ochterski, J.W., Martin, R.L., Morokuma, K., Farkas, O., Foresman, J.B., Fox, D.J., 2016. Gaussian 16, Revision A.03. Gaussian, Inc., Wallingford, CT.

Gómez-Zapata, P.A., Haelewaters, D., Quijada, L., Pfister, D.H., Aime, M.C., 2021. Notes on trochila (ascomycota, leotiomycetes), with new species and combinations. MycoKeys 78, 21–47. https://doi.org/10.3897/MYCOKEYS.78.62046.

Haga, A., Tamoto, H., Ishino, M., Kimura, E., Sugita, T., Kinoshita, K., Takahashi, K., Shiro, M., Koyama, K., 2013. Pyridone alkaloids from a marine-derived fungus, *stagonosporopsis cucurbitacearum*, and their activities against azole-resistant *Candida albicans*. J. Nat. Prod. 76, 750–754. https://doi.org/10.1021/np300876t.

Han, J., Liu, C., Li, L., Zhou, H., Liu, Li, Bao, L., Chen, Q., Song, F., Zhang, L., Li, E., Liu, Ling, Pei, Y., Jin, C., Xue, Y., Yin, W., Ma, Y., Liu, H., 2017. Decalin-containing tetramic acids and 4-Hydroxy-2-pyridones with antimicrobial and cytotoxic activity from the fungus *Coniochaeta cephalothecoides* collected in Tibetan Plateau (Medog). J. Org. Chem. 82, 11474–11486. https://doi.org/10.1021/acs.joc.7b02010.

Hardoim, P.R., van Overbeek, L.S., Berg, G., Pirttilä, A.M., Compant, S., Campisano, A., Döring, M., Sessitsch, A., 2015. The hidden world within plants: ecological and evolutionary considerations for defining functioning of microbial endophytes. Microbiol. Mol. Biol. Rev. 79, 293–320. https://doi.org/10.1128/mmbr.00050-14.

Homann, O.R., Dea, J., Noble, S.M., Johnson, A.D., 2009. A phenotypic profile of the *Candida albicans* regulatory network. PLoS Genet. 5, e1000783. https://doi.org/10.1371/journal.pgen.1000783.

Huelsenbeck, JP., Ronquist, F., 2001. MRBAYES: Bayesian inference of phylogenetic trees. Bioinformatics 17, 754–755. https://doi.org/10.1093/bioinformatics/17.8.754.

Ingólfsdóttr, K., 2002. Usnic acid. Phytochemistry 61, 729–736. https://doi.org/10.1016/S0031-9422(02)00383-7.

Jung, K.W., Yang, D.H., Maeng, S., Lee, K.T., So, Y.S., Hong, J., Choi, J., Byun, H.J., Kim, H., Bang, S., Song, M.H., Lee, J.W., Kim, M.S., Kim, S.Y., Ji, J.H., Park, G., Kwon, H., Cha, S., Meyers, G.L., Wang, L.L., Jang, J., Janbon, G., Adedoyin, G., Kim, T., Averette, A.K., Heitman, J., Cheong, E., Lee, Y.H., Lee, Y.W., Bahn, Y.S., 2015. Systematic functional profiling of transcription factor networks in Cryptococcus neoformans. Nat. Commun. 6, 6757. https://doi.org/10.1038/ncomms7757.

Kühbacher, A., Birch, M., Oliver, J.D., Gsaller, F., 2024. Anti- aspergillus activities of olorofim at sub-MIC levels during early-stage growth. Microbiol. Spectr. 12, e03304. https://doi.org/10.1128/spectrum.03304-23, 23.

Lee, J.C., Coval, S.J., Clardy, J., 1996. A cholesteryl ester transfer protein inhibitor from an insect-associated fungus. J ANTIBIOT 49, 693–696. https://doi.org/10.7164/antibiotics.49.693.

Nothias, L.-F., Petras, D., Schmid, R., Dührkop, K., Rainer, J., Sarvepalli, A., Protsyuk, I., Ernst, M., Tsugawa, H., Fleischauer, M., Aicheler, F., Aksenov, A.A., Alka, O., Allard, P.-M., Barsch, A., Cachet, X., Caraballo-Rodriguez, A.M., Da Silva, R.R., Dang, T., Garg, N., Gauglitz, J.M., Gurevich, A., Isaac, G., Jarmusch, A.K., Kameník, Z., Kang, K. Bin, Kessler, N., Koester, I., Korf, A., Le Gouellec, A., Ludwig, M., Martin, H.C., McCall, L.-I., McSayles, J., Meyer, S.W., Mohimani, H., Morsy, M., Moyne, O., Neumann, S., Neuweger, H., Nguyen, N.H., Nothias-Esposito, M., Paolini, J., Phelan, V.V., Pluskal, T., Quinn, R.A., Rogers, S., Shrestha, B., Tripathi, A., van der Hooft, J.J.J., Vargas, F., Weldon, K.C., Witting, M., Yang, H., Zhang, Z., Zubeil, F., Kohlbacher, O., Böcker, S., Alexandrov, T., Bandeira, N., Wang, M., Dorrestein, P.C., 2020. Feature-based molecular networking in the GNPS analysis environment. Nat. Methods 17, 905–908. https://doi.org/10.1038/s41592-020-0933-6.

Pluskal, T., Castillo, S., Villar-Briones, A., Orešič, M., 2010. MZmine 2: modular framework for processing, visualizing, and analyzing mass spectrometry-based molecular profile data. BMC Bioinf. 11, 395. https://doi.org/10.1186/1471-2105-11-395.

Rashid, M.A., Majid, M.A., Quader, M.A., 1999. Complete NMR assignments of (+)-usnic acid. Fitoterapia 70, 113–115. https://doi.org/10.1016/S0367-326X(98)00033-1.

Roca-Couso, R., Flores-Félix, J.D., Rivas, R., 2021. Mechanisms of action of microbial biocontrol agents against *Botrytis cinerea*. J. Fungi 7, 1045. https://doi.org/10.3390/jof7121045.

Schmid, R., Heuckeroth, S., Korf, A., Smirnov, A., Myers, O., Dyrlund, T.S., Bushuiev, R., Murray, K.J., Hoffmann, N., Lu, M., Sarvepalli, A., Zhang, Z., Fleischauer, M., Dührkop, K., Wesner, M., Hoogstra, S.J., Rudt, E., Mokshyna, O., Brungs, C., Ponomarov, K., Mutabdžija, L., Damiani, T., Pudney, C.J., Earll, M., Helmer, P.O., Fallon, T.R., Schulze, T., Rivas-Ubach, A., Bilbao, A., Richter, H., Nothias, L.F., Wang, M., Orešič, M., Weng, J.K., Böcker, S., Jeibmann, A., Hayen, H., Karst, U., Dorrestein, P.C., Petras, D., Du, X., Pluskal, T., 2023. Integrative analysis of multimodal mass spectrometry data in MZmine 3. Nat. Biotechnol. 41, 447–449. https://doi.org/10.1038/s41587-023-01690-2.

Shannon, P., Markiel, A., Ozier, O., Baliga, N.S., Wang J, T., Ramage, D., Amin, N., Schwikowski, B., Ideker, T., 2003. Cytoscape: a software environment for integrated models. Genome Res. 13, 426. https://doi.org/10.1101/gr.1239303.

Singh, B.K., Delgado-Baquerizo, M., Egidi, E., Guirado, E., Leach, J.E., Liu, H., Trivedi, P., 2023. Climate change impacts on plant pathogens, food security and paths forward. Nat. Rev. Microbiol. 21, 640–656. https://doi.org/10.1038/s41579-023-00900-7.

Sofianos, G., Samaras, A., Karaoglanidis, G., 2023. Multiple and multidrug resistance in Botrytis cinerea: molecular mechanisms of MLR/MDR strains in Greece and effects of co-existence of different resistance mechanisms on fungicide sensitivity. Front. Plant Sci. 14, 1273193. https://doi.org/10.3389/fpls.2023.1273193.

Wang, J., Wei, X., Qin, X., Lin, X., Zhou, X., Liao, S., Yang, B., Liu, J., Tu, Z., Liu, Y., 2015. Arthpyrones A-C, pyridone alkaloids from a sponge-derived fungus *Arthrinium arundinis* ZSDS1-F3. Org. Lett. 17, 656–659. https://doi.org/10.1021/ol503646c.

Witter, D.J., Vederas, J.C., 1996. Putative Diels−Alder-Catalyzed cyclization during the biosynthesis of lovastatin. J. Org. Chem. 61, 2613–2623. https://doi.org/10.1021/jo952117p.

Xu, M., Oppong-Danquah, E., Wang, X., Oddsson, S., Abdelrahman, A., Pedersen, S.V., Szomek, M., Gylfason, A.E., Snorradottir, B.S., Christensen, E.A., Tasdemir, D., Jameson, C.J., Murad, S., Andresson, O.S., Magnusson, K.P., de Boer, H.J., Thorsteinsdottir, M., Omarsdottir, S., Heidmarsson, S., Olafsdottir, E.S., 2022. Novel methods to characterise spatial distribution and enantiomeric composition of usnic acids in four Icelandic lichens. Phytochemistry 200, 113210. https://doi.org/10.1016/j.phytochem.2022.113210.

Zhang, Z., Jamieson, C.S., Zhao, Y., Li, D., Ohashi, M., Houk, K.N., Tang, Y., 2019. Enzyme-catalyzed inverse-electron demand diels–alder reaction in the biosynthesis of antifungal ilicicolin H. J. Am. Chem. Soc. 141 (14), 5659–5663. https://doi.org/10.1021/jacs.9b02204.